

A DISCONTINUOUS FINITE ELEMENT FORMULATION FOR HELMHOLTZ EQUATION

Gustavo Benitez Alvarez

Abimael Fernando Dourado Loula

benitez@lncc.br

aloc@lncc.br

National Laboratory of Scientific Computation – LNCC

Getulio Vargas 333 – Quitandinha – 25651-070 – Petrópolis, RJ, Brazil

Eduardo Gomes Dutra do Carmo

Fernando Alves Rochinha

carmo@lmn.con.ufrj.br

rochinha@adc.coppe.ufrj.br

COPPE – Federal University of Rio de Janeiro

Ilha do Fundão – 21945-970 – P.B. 68509 – Rio de Janeiro, RJ, Brazil

***Abstract.** The Helmholtz equation is a linear mathematical model that describes time-harmonic acoustic, elastic and electromagnetic waves. The finite element method is often used to obtain numerical solutions of the Helmholtz problem. It is well known that the performance of the Galerkin finite element method deteriorates for large values of the wave number k , due to the highly oscillatory behavior of the exact solution. In this paper a finite element formulation with discontinuous interpolations across interelements boundaries is presented for Helmholtz problem. The proposed formulation introduces two parameters β and λ that should be chosen appropriately. We chose both parameters by numerical experiments. The accuracy and stability of the proposed formulation for the linear and bilinear shape functions is demonstrated in several numerical examples in one and two-dimensions.*

***Keywords:** Stabilized FEM, Discontinuous Galerkin, Helmholtz equation, discontinuous finite element method*

1. INTRODUCTION

The Helmholtz equation is the linear mathematical model that describes time-harmonic acoustic, elastic and electromagnetic waves. The finite element method is often used to obtain numerical solutions of the Helmholtz problem. The oscillatory behavior of the exact solution and the quality of the approximate numerical solution depends on the wave number k . The resolution of the mesh n_{res} should be adjusted to the wave number according to a "rule of the thumb" $n_{res} = \frac{\Lambda}{h} = \frac{2\pi}{kh}$, where Λ is the wave-length and h is the element diameter of the mesh (Harari and Hughes, 1991).

The rule of thumb controls the interpolation error. For low waves number the approximate solution of the classic finite element method guarantee a reasonable result (Bayliss et al., 1985). However, the performance of the Galerkin finite element method is deteriorated when k is increased and the error of the finite element approximation grows with the wave number even when the rule of thumb is observed. This is known as the pollution of the finite element solution. The errors in H' -norm are bounded only if the mesh resolution is appropriately increased: $kh \ll 1$ in the preasymptotic range (Ihlenburg and Babuška, 1995) and $k^2h \ll 1$ in the asymptotic range of convergence (Douglas et al., 1993 and Harari et al., 1992,). The pollution effect can only be avoided after a drastic refinement of the mesh. This obviously impedes the numerical analyses of the Helmholtz equation by the finite element method in mid and high frequency.

A great variety of stabilized finite element formulations have been developed to alleviate the pollution effect (Babuška et al., 1995, Thompson et al., 1995, Ihlenburg et al., 1997 and Franca et al., 1997). The relative merits of some of these formulations are presented in Farhat et al. (2003).

In this work we apply the discontinuous finite element formulation developed in Do Carmo et al. (2002) to the Helmholtz equation. The formulation shows excellent properties of stability and accuracy, both for one-dimensional or two-dimensional problems.

2. THE HELMHOLTZ EQUATION

2.1 The boundary value problem

Let $\Omega \subset R^n$ be an open bounded domain, whose boundary Γ is a piecewise smooth boundary. The unit outward normal vector \hat{n} to Γ is defined almost everywhere. We shall consider the problem:

$$-\nabla \cdot (\nabla u) - k^2 u = f \quad \text{in } \Omega, \quad (1)$$

$$u = g \quad \text{on } \Gamma_g, \quad (2)$$

$$\nabla u \cdot \hat{n} = q \quad \text{on } \Gamma_q, \quad (3)$$

$$\nabla u \cdot \hat{n} + \alpha u = r \quad \text{on } \Gamma_r, \quad (4)$$

where u denotes the unknown field, k is the wave number, f is the volume source term and g , q and r are the boundary conditions prescribed for the problem.

2.2 Variational Formulation

Consider the set of all functions S and the space of the admissible variations V defined as: $S = \{u \in H^1(\Omega) : u = g \text{ on } \Gamma_g\}$, $V = \{v \in H^1(\Omega) : v = 0 \text{ on } \Gamma_g\}$, where $H^1(\Omega)$ is the

standard Hilbert space. The variational formulation of the boundary value problem defined as Eq. (1) to Eq. (4), involves finding $u \in S$ that satisfies the variational equation:

$$\int_{\Omega} [(\nabla u) \cdot \nabla v - k^2 uv] d\Omega - \int_{\Gamma_q} qv d\Gamma_q + \int_{\Gamma_r} (\alpha u - r)v d\Gamma_r = \int_{\Omega} f v d\Omega \quad \forall v \in V. \quad (5)$$

2.3 Finite element formulations

Consider $M^h = \{\Omega_1, \dots, \Omega_{ne}\}$ a finite element partition of Ω , such that: $\bar{\Omega} = \bigcup_{e=1}^{ne} \bar{\Omega}_e$, $\bar{\Omega} = \Omega \cup \Gamma$, $\bar{\Omega}_e = \Omega_e \cup \Gamma_e$ and $\Omega_e \cap \Omega_{e'} = \emptyset$ if $e \neq e'$. The respective finite element set and space of S and V are defined as: $S^{h,l} = \{u^h \in H^1(\Omega) : u_e^h \in P^l(\Omega_e), u^h = g^h \text{ on } \Gamma_g\}$ and $V^{h,l} = \{v^h \in H^1(\Omega) : v_e^h \in P^l(\Omega_e), v^h = 0 \text{ on } \Gamma_g\}$, where $P^l(\Omega_e)$ is the space of polynomials of degree l , g^h denotes the interpolation of g and u_e^h denotes the restriction of u^h to Ω_e .

Problem Eq. (5) have been approximated by the following finite element methods: find $u^h \in S^{h,l}$ that satisfies $\forall v^h \in V^{h,l}$,

Galerkin method

$$A_G(u^h, v^h) = F_G(v^h), \quad (6)$$

$$A_G = \sum_{e=1}^{ne} \int_{\Omega_e} [\nabla u_e^h \cdot \nabla v_e^h - k^2 u_e^h v_e^h] d\Omega_e, \quad F_G = \sum_{e=1}^{ne} \int_{\Omega_e} f v_e^h d\Omega_e, \quad (7)$$

Galerkin + Least-Squares method (GLS)

$$A_G(u^h, v^h) + A_{LS}(u^h, v^h) = F_G(v^h) + F_{LS}(v^h), \quad (8)$$

$$A_{LS} = \sum_{e=1}^{ne} \int_{\Omega_e} [-\nabla \cdot (\nabla u_e^h) - k^2 u_e^h] p_e^h d\Omega_e, \quad F_{LS} = \sum_{e=1}^{ne} \int_{\Omega_e} f_e p_e^h d\Omega_e, \quad (9)$$

$$p_e^h = \tau_e [-\nabla \cdot (\nabla v_e^h) - k^2 v_e^h] \quad \forall \Omega_e \in M^h, \quad (10)$$

$$\tau_e = \frac{1}{k^2} \left[1 - 6 \frac{4 - \cos \zeta_1 - \cos \zeta_2 - 2 \cos \zeta_1 \cos \zeta_2}{(2 + \cos \zeta_1)(2 + \cos \zeta_2) k^2 h^2} \right], \quad \zeta_1 = kh \cos \theta, \quad \zeta_2 = kh \sin \theta. \quad (11)$$

In one dimension with appropriate choice of τ this GLS finite element approximation coincide with the nodal interpolant. In two dimensions the parameter τ depends on the direction of the wave, which in most of the cases of interest is unknown. For this reason, the solution of GLS presents a strong dependence on the direction of the wave and its error can be of the order of Galerkin's error.

3. A DISCONTINUOUS FINITE ELEMENT METHOD

3.1 Differential form of the boundary value problem by subdomain

Defining $H(\Omega, M^h) = \{\psi \in L^2(\Omega) : \psi_e \in H^1(\Omega_e) \text{ and } \nabla \cdot (\nabla \psi_e) \in L^2(\Omega_e)\}$, $S_{DG} = \{u \in H(\Omega, M^h) : u = g \text{ on } \Gamma_g\}$ and $V_{DG} = \{v \in H(\Omega, M^h) : v = 0 \text{ on } \Gamma_g\}$. We present the Helmholtz problem by subdomains as follows: find $u \in H(\Omega, M^h)$ satisfying

$$-\nabla \cdot (\nabla u_e) - k_e^2 u_e = f_e \quad \text{in } \Omega_e, \quad (12)$$

$$u_e = g_e \quad \text{on } \Gamma_g \cap \Gamma_e \neq \emptyset, \quad (13)$$

$$\nabla u_e \cdot \hat{n}_e = q_e \quad \text{on } \Gamma_q \cap \Gamma_e \neq \emptyset, \quad (14)$$

$$\nabla u_e \cdot \hat{n}_e + \alpha_e u_e = r_e \quad \text{on } \Gamma_r \cap \Gamma_e \neq \emptyset. \quad (15)$$

3.2 Equivalent variational formulation

We introduce a family of variational formulations to the subdomain differential form (12-15) as: find $u \in S_{DG}$ that satisfies:

$$A_G(u, v) + A_{DG}(u, v) = F_G(v) \quad \forall v \in V_{DG}, \quad (16)$$

$$A_{DG} = \sum_{\substack{e' > e \\ \Gamma_{ee'} \neq \emptyset}}^{ne} \int_{\Gamma_{ee'}} \left[\frac{\beta^{ee'}}{h_{ee'}} (u_e - u_{e'}) (v_e - v_{e'}) + \frac{\lambda^{ee'}}{2} (u_e - u_{e'}) (\nabla v_e \cdot \hat{n}_e - \nabla v_{e'} \cdot \hat{n}_{e'}) \right. \\ \left. - \frac{1}{2} (\nabla u_e \cdot \hat{n}_e - \nabla u_{e'} \cdot \hat{n}_{e'}) (v_e - v_{e'}) \right] d\Gamma_{ee'}, \quad (17)$$

$$h_{ee'} = \min\{h_e, h_{e'}\}, \quad (18)$$

where, $\beta^{ee'}$ and $\lambda^{ee'}$ are functions that will be determined latter. For more details on this kind of variational formulation see Do Carmo et al. (2002). Also, in Do Carmo et al. (2002) we find results about existence and uniqueness, and the continuity of the solution with respect to the data, for elliptic problems, where $\beta^{ee'}$ and $\lambda^{ee'}$ should be chosen as $\beta^{ee'} \geq \beta_o > 0$ and $-1 \leq \lambda^{ee'} \leq 1$. These restrictions for $\beta^{ee'}$ and $\lambda^{ee'}$ are not valid in the case of Helmholtz equation, which is not elliptic for high values of k .

3.3 The finite element approximation

Introducing the discontinuous finite element spaces of degree $l \geq 1$ $S_{DG}^{h,l} = \{u \in L^2(\Omega) : u_e \in P^l(\Omega_e) \text{ and } u = g^h \text{ on } \Gamma_g\}$, $V_{DG}^{h,l} = \{v \in L^2(\Omega) : v_e \in P^l(\Omega_e) \text{ and } v = 0 \text{ on } \Gamma_g\}$, with g^h the usual interpolation of g , the corresponding finite element formulation consists in finding $u^h \in S_{DG}^{h,l}$ satisfying:

$$A_G(u^h, v^h) + A_{DG}(u^h, v^h) = F_G(v^h) \quad \forall v^h \in V_{DG}^{h,l}. \quad (19)$$

The above formulation is in fact a family of methods parameterized by the pair β and λ . For strongly elliptic problems, β and λ are determined by a priori error estimates, but for the Helmholtz equation this estimate is not valid anymore. Thus, we will determine optimal β and λ through numerical experiments, and we assumed that β and λ are functions of two dimensionless parameters: kh and kL .

4. NUMERICAL RESULTS

In this section, we first determined optimal values for β and λ through numerical experiments carried out on a one-dimensional model problem. Then, using β and λ previously determined, we solved other problems to illustrate the performance of the proposed

discontinuous finite element method. In all cases, we used linear and bilinear shape functions and exact 2 or 2x2 Gaussian integration.

4.1 Numerical determination of the β and λ functions

For each choice of β and λ we have a discontinuous finite element solution $u_{DG}^h(\beta, \lambda)$. We look for β and λ such that the relative errors in the L^2 -norm and H^1 -seminorm are minimized in a set of numerical experiments for the Helmholtz problem in one-dimension and uniform meshes. These optimal values, which are not restricted to a single pair, will be used in more general situations, that is, two-dimensional case and uniform meshes.

Let us consider the problem given by the equation (1) in one dimension with $k^2=\text{constant}$, $f(x)=0$ and Dirichlet boundary conditions: $u(0)=1$ and $u(1)=\cos(k)$. In this case, the exact solution of the problem is $u_{ex}(x)=\cos(kx)$. The errors in the L^2 -norm and H^1 -seminorm are functional of β and λ given by

$$\|E_{DG}(\beta, \lambda)\|_{L^2(\Omega)} = \|u_{ex} - u_{DG}^h(\beta, \lambda)\|_{L^2(\Omega)} = \left[\sum_{e=1}^{ne} \int_{\Omega_e} (u_{ex} - u_{DG}^{h,e}(\beta, \lambda))^2 d\Omega_e \right]^{\frac{1}{2}},$$

$$|E_{DG}(\beta, \lambda)|_{H^1(\Omega)} = |u_{ex} - u_{DG}^h(\beta, \lambda)|_{H^1(\Omega)} = \left[\sum_{e=1}^{ne} \int_{\Omega_e} \left(\frac{du_{ex}}{dx} - \frac{du_{DG}^{h,e}(\beta, \lambda)}{dx} \right)^2 d\Omega_e \right]^{\frac{1}{2}},$$

and the corresponding relative error are

$$\|RE_{DG}(\beta, \lambda)\|_{L^2(\Omega)} = \frac{\|E_{DG}(\beta, \lambda)\|_{L^2(\Omega)}}{\|u_{ex}\|_{L^2(\Omega)}}, \quad |RE_{DG}(\beta, \lambda)|_{H^1(\Omega)} = \frac{|E_{DG}(\beta, \lambda)|_{H^1(\Omega)}}{|u_{ex}|_{H^1(\Omega)}}.$$

In Figure 1 we show $\|RE_{DG}(\beta, \lambda)\|_{L^2(\Omega)}$ and $|E_{DG}(\beta, \lambda)|_{H^1(\Omega)}$ as a function of β e λ obtained with a uniform mesh of 40 elements. To assess the performance of the proposed method we use for comparison the relative error in the L^2 -norm of the interpolant ($RE_I=0.0207$) and of the continuous Galerkin finite element solution ($RE_{CG}=0.125$). For some regions of the $\beta\lambda$ plane, the accuracy of the discontinuous solution is quite similar to the interpolant, which can be considered as target to any finite element method. It is important to highlight that those regions encompass positive and/or negative values of the parameters. Similar conclusion can be drawn from Figure 1 (b) that depicts H^1 semi-norm of the error. The only point to be mention is that in this last case the regions of good performance are larger. In Figure 2, we carry out the same study for a higher wave number, $k^2=4000$, for which 160 elements were used. Observing Figures 1 and 2 we note that as the wave number k increases the region of optimal choice, in the $\beta\lambda$ plane, in which the error of the DG approximation is close to the error of the interpolant, becomes narrower.

Restricting our search for optimal values to the region where β and λ are positive, the numerical experiments indicate that β_{res} and λ_{res} (the optimal values for those functions) depend on two dimensionless parameters $\mu_1 = k_e \bar{h}_{ee'}$ and $\mu_2 = k_e L$, where $\bar{h}_{ee'} = \min\{h_i^e, h_i^{e'}\}$, $h_i^e = \max_{x,y \in \Omega_e} |x_i - y_i|$, $h_i^{e'} = \max_{x,y \in \Omega_{e'}} |x_i - y_i|$ and $L = \max\{L_i\}$, $L_i = \max_{x,y \in \Omega} |x_i - y_i|$ ($i=1, \dots$, domain dimension).

The dependence of the optimal values on μ_1 and μ_2 is initially investigated by fixing the former ($\mu_1 = \frac{\pi}{5} \approx 0.628$) and plotting both β_{res} and λ_{res} as functions of the second in Figure 3.

The curve presented in that figure is divided in three regions, which leads to the following interpolation using Lagrange polynomials:

$$\lambda_{res} = \begin{cases} \sum_{i=1}^2 C_{\lambda}^1(i)\eta_i(\xi), & \bar{\mu}_2 = 20.5, \quad \Delta\mu_2 = 39 \quad \text{if } 1 \leq \mu_2 \leq 40 \\ \sum_{i=1}^6 C_{\lambda}^2(i)\eta_i(\xi), & \bar{\mu}_2 = 160, \quad \Delta\mu_2 = 240 \quad \text{if } 40 < \mu_2 \leq 280 \\ \sum_{i=1}^2 C_{\lambda}^3(i)\eta_i(\xi), & \bar{\mu}_2 = 650, \quad \Delta\mu_2 = 740 \quad \text{if } 280 < \mu_2 \leq 1020 \end{cases}, \quad (20)$$

$$\beta_{res} = \begin{cases} \sum_{i=1}^2 C_{\beta}^1(i)\eta_i(\xi), & \bar{\mu}_2 = 20.5, \quad \Delta\mu_2 = 39 \quad \text{if } 1 \leq \mu_2 \leq 40 \\ \sum_{i=1}^6 C_{\beta}^2(i)\eta_i(\xi), & \bar{\mu}_2 = 160, \quad \Delta\mu_2 = 240 \quad \text{if } 40 < \mu_2 \leq 280 \\ \sum_{i=1}^2 C_{\beta}^3(i)\eta_i(\xi), & \bar{\mu}_2 = 650, \quad \Delta\mu_2 = 740 \quad \text{if } 280 < \mu_2 \leq 1020 \end{cases}, \quad (21)$$

where $\xi = \frac{2}{\Delta\mu_2}(\mu_2 - \bar{\mu}_2)$ and $\eta_i(\xi)$ are the usual Lagrange polynomial. We should highlight that although $\mu_2 = 1020$ was used as superior limit to calculate the coefficients, Figure 3 indicates that bigger values of μ_2 should verify the same linear dependence. The coefficients $C_{\lambda}^j(i)$ and $C_{\beta}^j(i)$ are determined by least squares fitting and presented in Table 1. To find the dependence of β and λ with μ_1 , we define the following functions:

$$Pol(\mu_1) = \frac{\lambda / \lambda_{res}}{\beta / \beta_{res}}, \quad (22)$$

$$\beta(\mu_1, \mu_2) = \beta_{res}(\mu_2) f_{\beta}(\mu_1), \quad (23)$$

$$\lambda(\mu_1, \mu_2) = \lambda_{res}(\mu_2) f_{\lambda}(\mu_1) = \lambda_{res}(\mu_2) f_{\beta}(\mu_1) Pol(\mu_1), \quad (24)$$

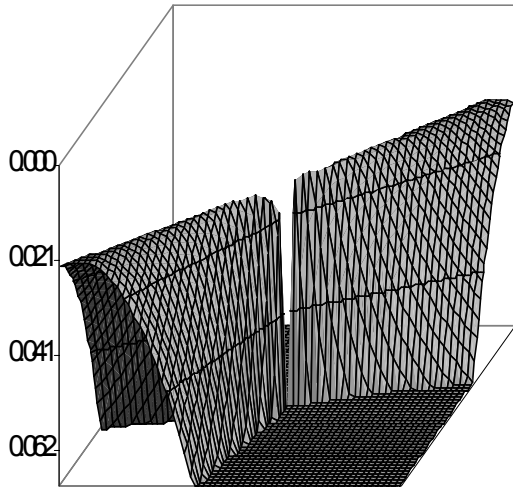
where $Pol(\mu_1)$ and $f_{\beta}(\mu_1)$ are fitted by Lagrange's polynomial through numerical experiments. The numerical tests showed that the degree of polynomial larger than 2 for $Pol(\mu_1)$ and larger than 4 for $f_{\beta}(\mu_1)$ had very little influence on the relative error in L²-norm. Therefore, the numerical experiments determined $Pol(\mu_1)$ and $f_{\beta}(\mu_1)$ as:

$$Pol(\mu_1) = \sum_{i=1}^3 C_p(i)\eta_i(\xi), \quad \bar{\mu}_1 = 0.33148806, \quad \Delta\mu_1 = 0.60018177, \quad (25)$$

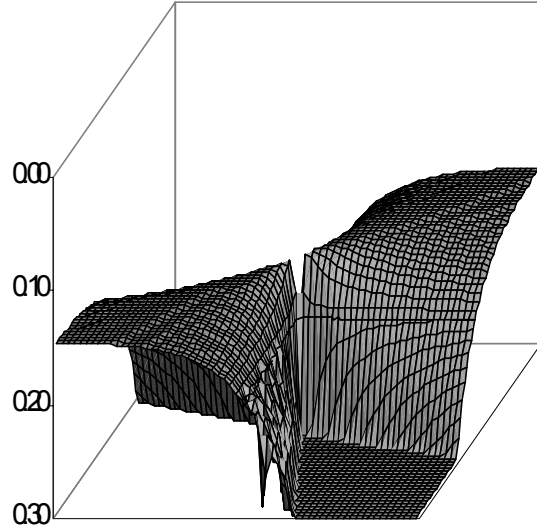
$$f_{\beta}(\mu_1) = \sum_{i=1}^5 C_{f\beta}(i)\eta_i(\xi), \quad \bar{\mu}_1 = 0.33148806, \quad \Delta\mu_1 = 0.60018177. \quad (26)$$

Table 1: Coefficients determined by least squares fitting.

i	C_{λ}^1	C_{λ}^2	C_{λ}^3	C_{β}^1	C_{β}^2	C_{β}^3	C_p	$C_{f\beta}$
1	0.88562	10.71380	24.43120	10.60911	11.68891	24.93120	1.04353	9.28141
2	10.86634	20.85016	25.72949	12.03286	21.30053	26.22949	0.97743	2.22206
3	-	21.75043	-	-	22.27510	-	1.00022	2.01088
4	-	22.92634	-	-	23.42139	-	-	7.28845
5	-	23.83735	-	-	24.32916	-	-	0.51209
6	-	24.11425	-	-	24.60180	-	-	-

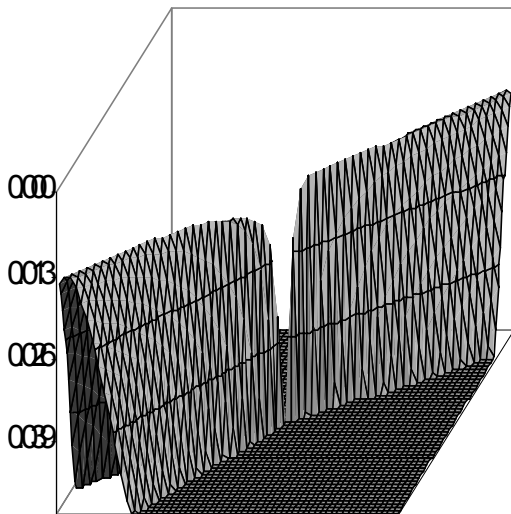


(a) REi=0.0207, REcg=0.125

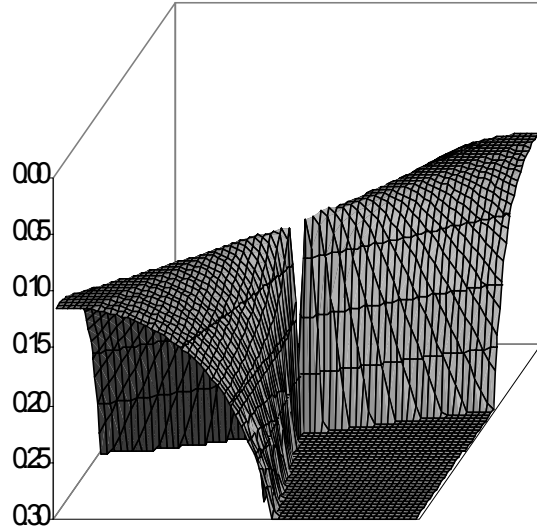


(b) REi=0.146, REcg=0.193

Figure 1. Relative error RE_{DG} in the L^2 -norm (case-a) and H^1 -seminorm (case-b) for $k^2=400$:
 $ne=40, -300 \leq \beta, \lambda \leq 300, \Delta\beta=10, \Delta\lambda=10$.



(a) REi=0.0129, REcg=8.96



(b) REi=0.114, REcg=9.02

Figure 2. Relative error RE_{DG} in the L^2 -norm (case-a) and H^1 -seminorm (case-b) for $k^2=4000$:
 $ne=160, -300 \leq \beta, \lambda \leq 300, \Delta\beta=10, \Delta\lambda=10$.

In Figures 4 and 5 we plot the relative errors of CG and DG approximations as a function of dimensionless parameter $B = k^2 h^2$ for three values of k . In both figures the curves E_I correspond to the error of the nodal interpolant. In each case, the β and λ functions are determined by (20-26). In Figure 4 we can observe clearly the pollution effect when k is increased. In this case, the critical number of degrees of freedom (DOF) for the Galerkin finite element error is predicted by $N_{DOF} = \sqrt{\frac{k^3}{24}}$ whereas that for the nodal interpolant by $N_{DOF} = \frac{k}{\pi}$. Also, the Galerkin FE error is not controlled by the magnitude of kh . Observing

Figure 5 we can verify that the error behavior of the nodal interpolant and discontinuous FE solution are very close for the different k . It is well known that the nodal interpolation error satisfies the following estimates if $u \in H^2(\Omega)$:

$$\frac{\|u_{ex} - u_I^h\|_{L^2(\Omega)}}{\|u_{ex}\|_{L^2(\Omega)}} \leq C_1 k^2 h^2, \quad \frac{|u_{ex} - u_I^h|_{H^1(\Omega)}}{|u_{ex}|_{H^1(\Omega)}} \leq C_2 kh,$$

where C_1 and C_2 are constants not depending on k and h . It was numerically determined that starting from certain value $B=B_0$ the following expressions are verified for the nodal interpolation error and the discontinuous FE error:

$$\frac{\|u_{ex} - u_I^h\|_{L^2(\Omega)}}{\|u_{ex}\|_{L^2(\Omega)}} = C_{1I} (k^2 h^2)^{A_{1I}}, \quad \frac{|u_{ex} - u_I^h|_{H^1(\Omega)}}{|u_{ex}|_{H^1(\Omega)}} = C_{2I} (k^2 h^2)^{A_{2I}},$$

$$\frac{\|u_{ex} - u_{DG}^h\|_{L^2(\Omega)}}{\|u_{ex}\|_{L^2(\Omega)}} = C_{1DG} (k^2 h^2)^{A_{1DG}}, \quad \frac{|u_{ex} - u_{DG}^h|_{H^1(\Omega)}}{|u_{ex}|_{H^1(\Omega)}} = C_{2DG} (k^2 h^2)^{A_{2D}},$$

with the parameters introduced above shown in Table 2.

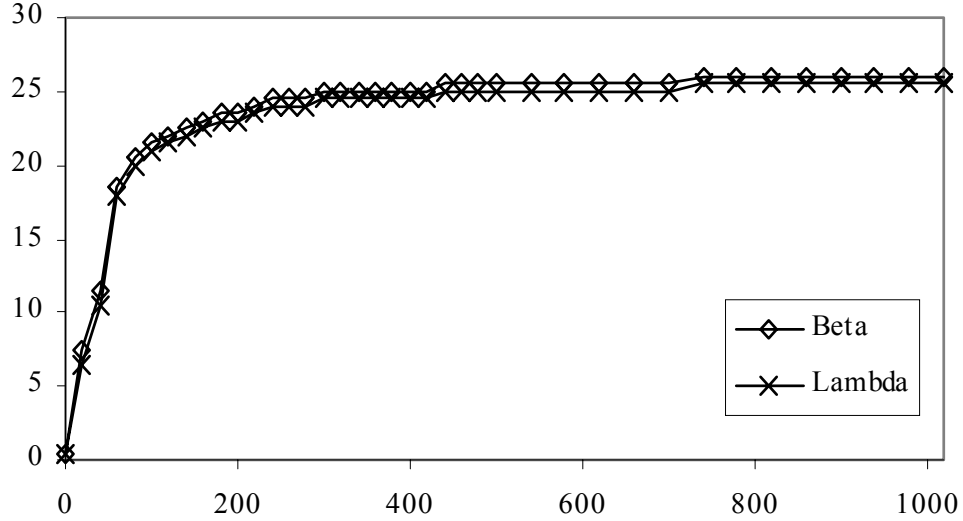


Figure 3. Dependence of β_{res} and λ_{res} with μ_2 .

Table 2: Convergence rates determined by numerical experiments.

k^2	C_{1I}	A_{1I}	C_{2I}	A_{2I}	C_{1DG}	A_{1DG}	C_{2DG}	A_{2DG}
400	0.0831	0.99966	0.2937	0.49981	0.0831	0.99976	0.2937	0.49981
4000	0.0828	0.99886	0.2893	0.49932	0.0875	1.01032	0.2896	0.49948
40000	0.0827	0.99777	0.2867	0.49865	0.0830	0.99877	0.2867	0.49868

In Figs. 6, 7 and 8 show some solutions in one-dimension for $k^2=400$, 4000 and 40000. The exact solution is also plotted. All results up to now are obtained using β and λ given by (20-26). As expected, we observe spurious dispersion of the continuous method, this degradation of the solution quality is a manifestation of the pollution effect. It is important to reinforce that the proposed method has achieved for coarser meshes better results, being able to capture the correct phase and amplitude.

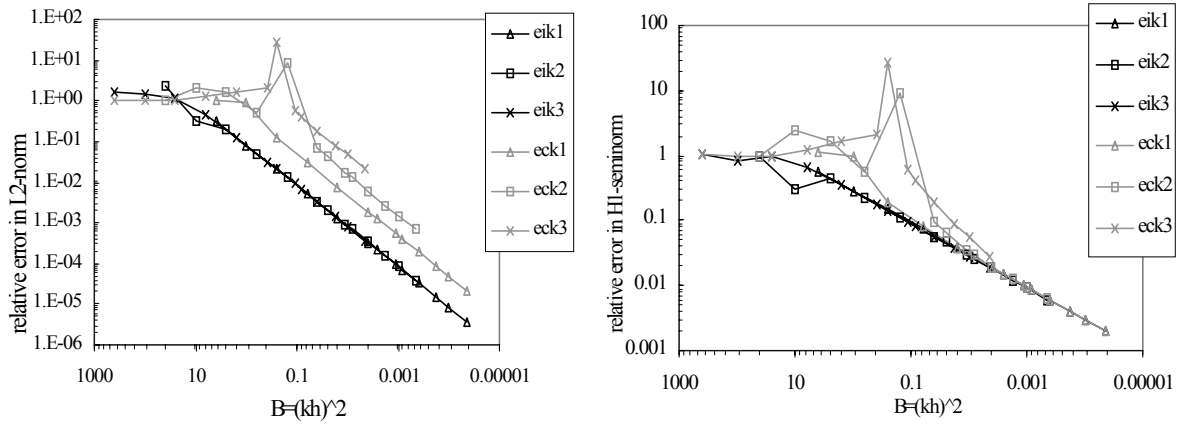


Figure 4. Relative errors RE_{CG} and RE_I for $k^2=400, 4000, 40000$: (a) the L^2 -norm and (b) H^1 -seminorm.

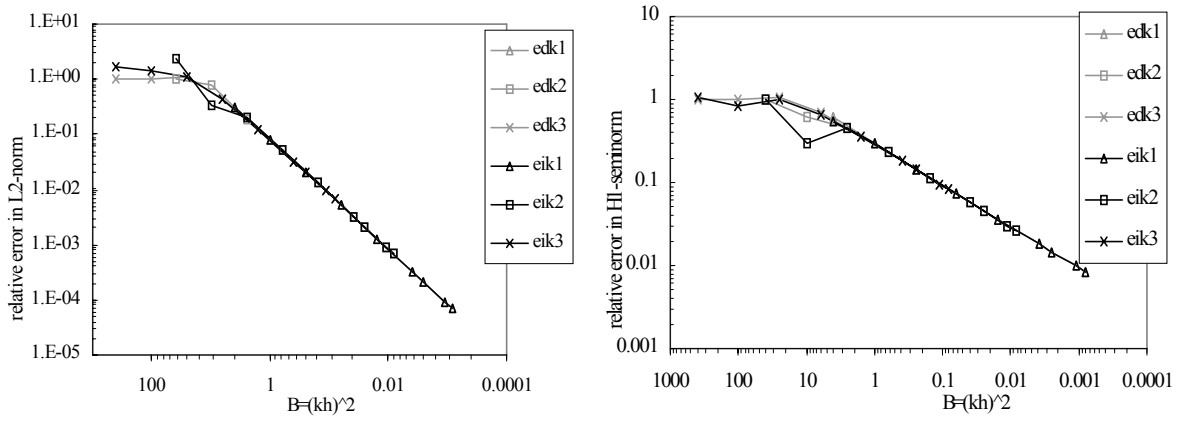
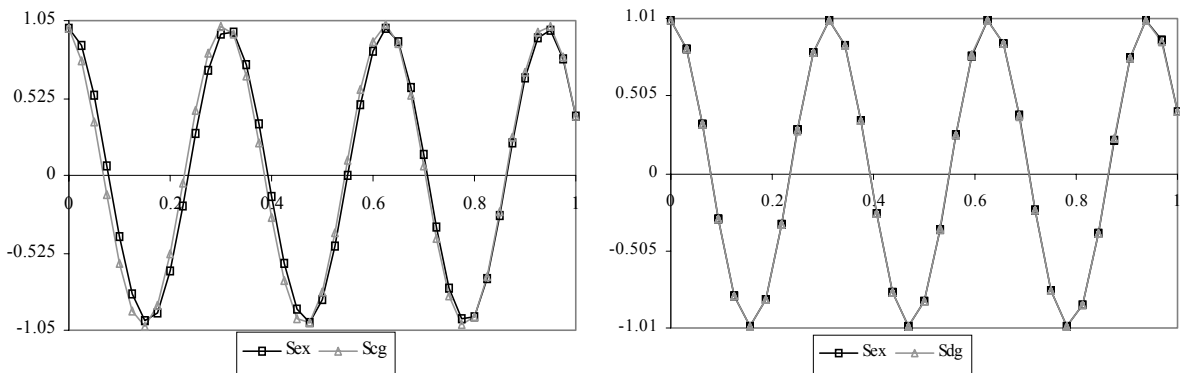


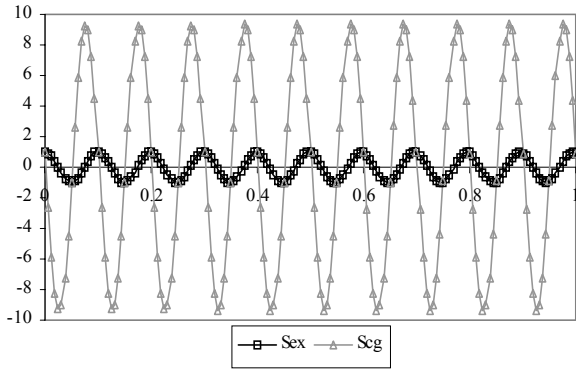
Figure 5. Relative errors RE_{DG} and RE_I for $k^2=400, 4000, 40000$: (a) the L^2 -norm and (b) H^1 -seminorm.



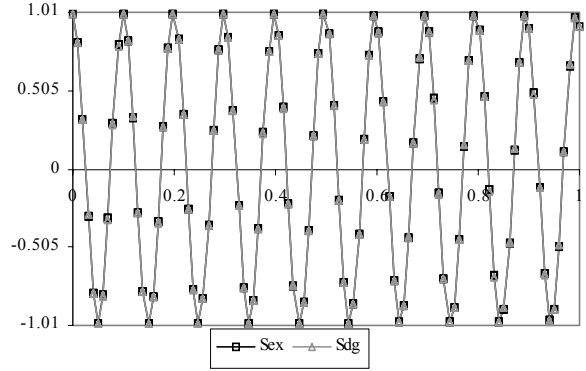
(a) Galerkin FE solution $kh=0.5$

(b) Discontinuous FE solution $kh=0.625$

Figure 6. Solution of homogeneous problem in one dimension $k^2=400$

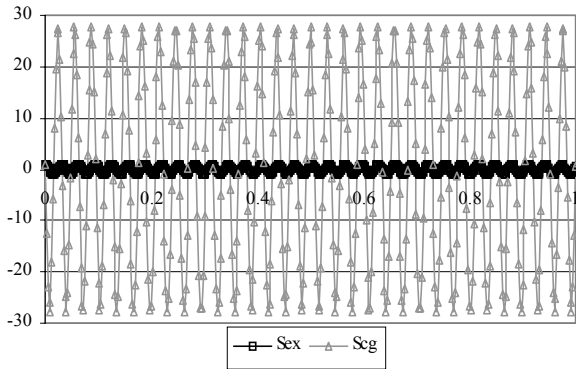


(a) Galerkin FE solution $kh=0.395$

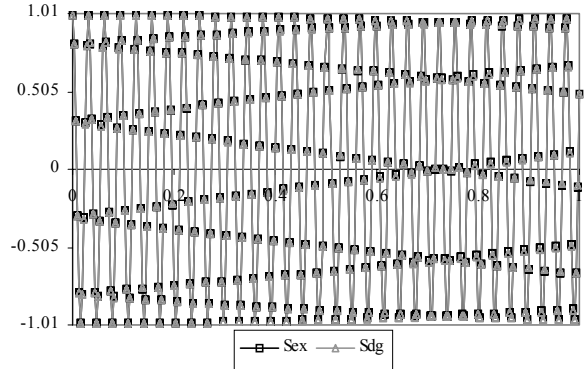


(b) Discontinuous FE solution $kh=0.626$

Figure 7. Solution of homogeneous problem in one dimension $k^2=4000$



(a) Galerkin FE solution $kh=0.5$



(b) Discontinuous FE solution $kh=0.627$

Figure 8. Solution of homogeneous problem in one dimension $k^2=40000$

4.2 Dispersion analysis

Now we face a more challenging situation concerning the propagation of a plane wave in an arbitrary direction not necessarily aligned to the mesh. It is important to mention that the propagation direction is usually not known a priori. This more general situation is decisive to examine the dispersion properties of the proposed discontinuous finite element formulation. We consider the problem given by equation (1) in a square domain of unity sides, $k^2=constant$, $f(x,y)=0$ and the following Dirichlet boundary conditions: $u(0,y)=\cos(k(y\sin\theta))$, $u(1,y)=\cos(k(\cos\theta+y\sin\theta))$, $u(x,0)=\cos(k(x\cos\theta))$, and $u(x,1)=\cos(k(x\cos\theta+y\sin\theta))$. The exact solution of this problem is the real part of a plane wave propagating in the θ -direction in two dimension: $u(x,y)=\cos(k(x\cos\theta+y\sin\theta))$. In the experiments this propagation direction varies in the range $0 \leq \theta \leq \frac{\pi}{2}$.

Figures 9 and 10 presents the relative errors of discontinuous FE solution (Edg) compared to the nodal interpolant (Ei), Galerkin FEM (Ecg) and GLS ($Egls$) solutions in the L^2 -norm as a function of θ -direction for two uniform meshes and different values of the wave number k . E_i , E_{gls} and E_{cg} corresponds to the relative errors of the nodal interpolant, GLS and the Galerkin FE solutions respectively. In case (a) the mesh is coarse ($kh>0.62$), case (b) the mesh verifies the rule of thumb $kh=\pi/5\approx 0.62$. In choosing β and λ we adopt two strategies. First β_{res} and λ_{res} values are determined by (20-26) (E_{dg1}). Second β and λ are chosen such that $\beta_1=10^5 \gg \beta_{res}$ and $\lambda_1=108685 \gg \lambda_{res}$ (E_{dg2}). We observe that whenever the mesh verifies the rule of thumb (case b) starting from $\beta=\beta_{res}$ and $\lambda=\lambda_{res}$, we can chose $\beta \gg \beta_{res}$ and $\lambda \gg \lambda_{res}$

keeping a relationship between them, such what equivalent results are obtained. It is to say, β and λ belong to the region where the functional of the errors in L^2 -norm and H^1 -seminorm attains its minimum. For the coarse mesh (case a) the previous statement is not valid as show the Figures 9(a) and 10(a). In this case, it is necessary what $\beta < \beta_{res}$ and $\lambda < \lambda_{res}$ to get the relative error of the discontinuous FE solution close the relative error of the nodal interpolant.

In Figure 11 we plot the nodal interpolant, discontinuous FE and Galerkin FE solutions in sections $x=0.505$ (case a) and $y=0.505$ (case b), respectively along x and y directions. The results were obtained with (101×101) mesh for $\theta = ((3\pi)/8)$, that is the θ -direction, which corresponds to the greatest "phase" error. The β and λ functions are, once again, chosen by using (20-26). Those results confirm the good performance of the proposed method.

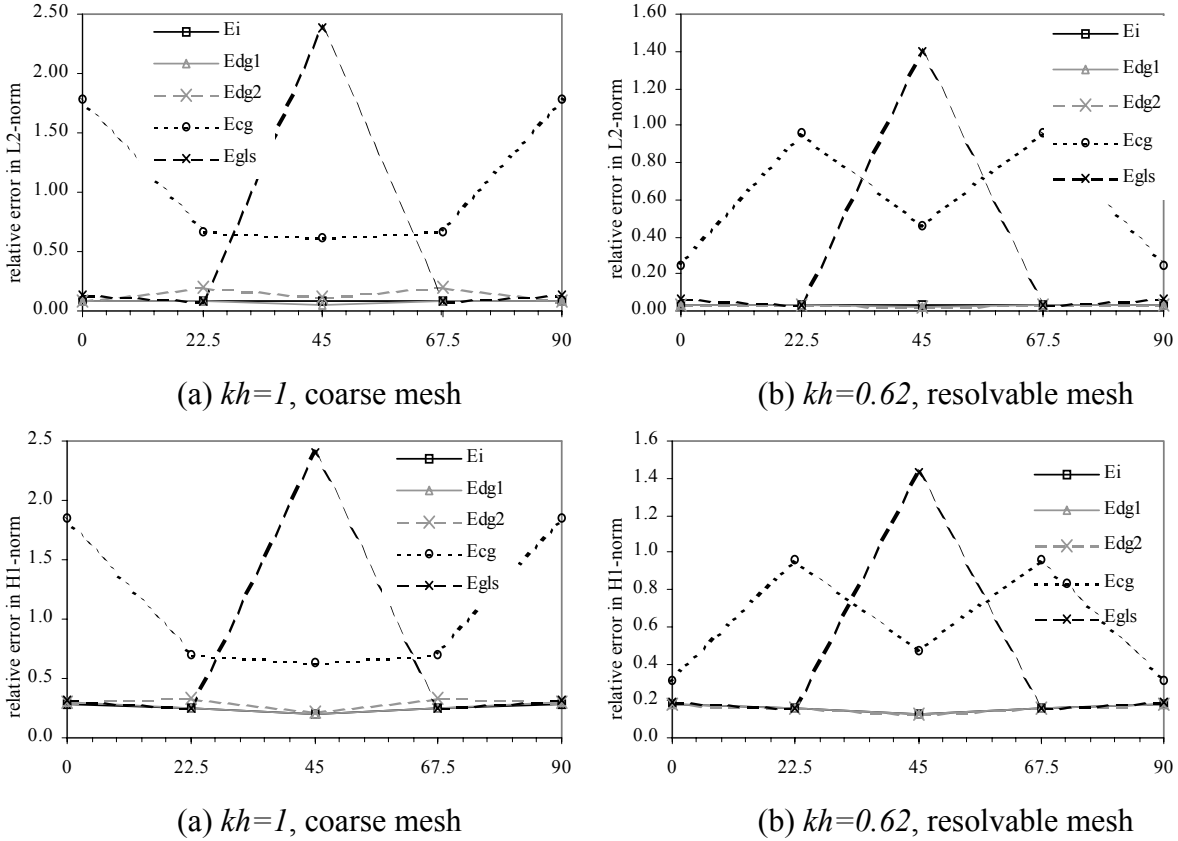
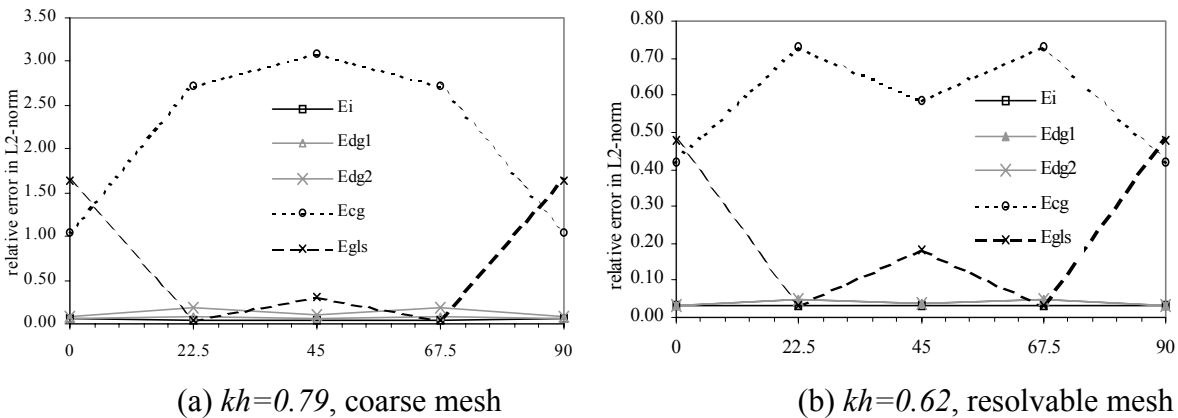
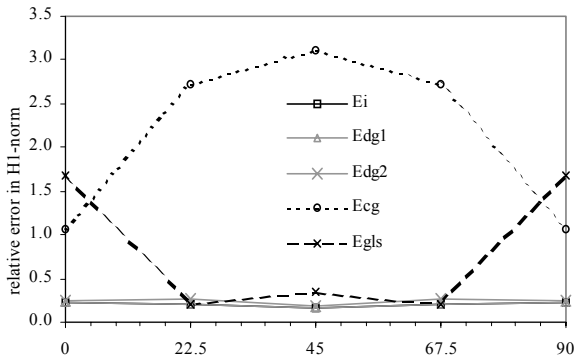
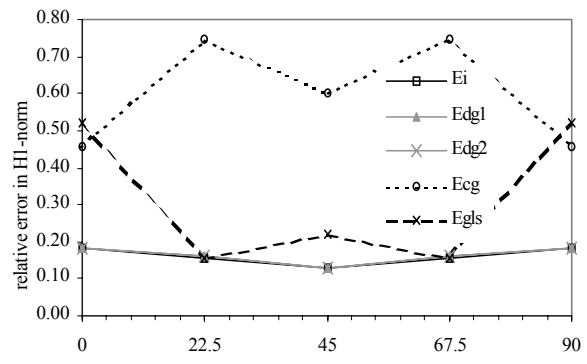


Figure 9. Relative errors of the DFE solution (RE_{DG}) compared to the nodal interpolant (RE_I) in the L^2 -norm and H^1 -norm as a function of θ -direction: $k^2=400$.



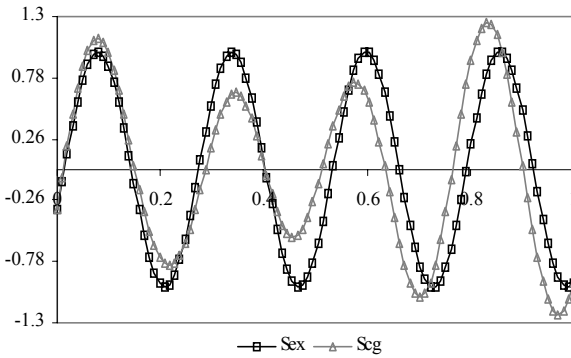


(a) $kh=0.79$, coarse mesh

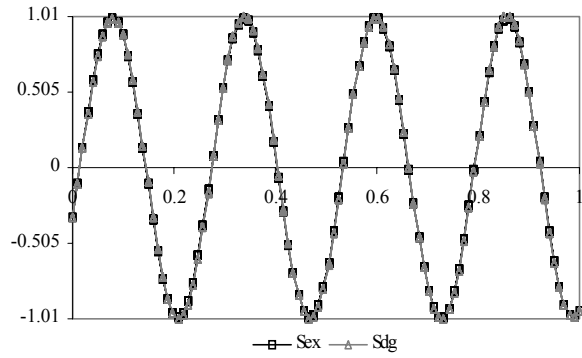


(b) $kh=0.62$, resolvable mesh

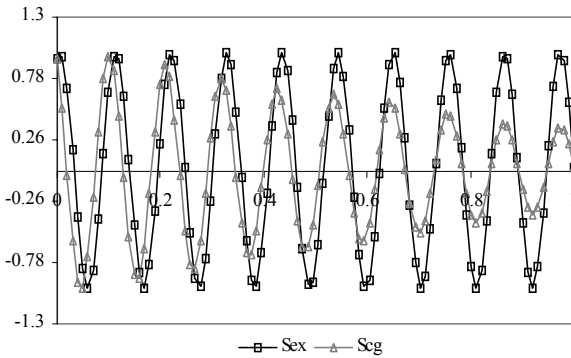
Figure 10. Relative errors of the DFE solution (RE_{DG}) compared to the nodal interpolant (RE_I) in the L^2 -norm and H^1 -norm as a function of θ -direction: $k^2=4000$.



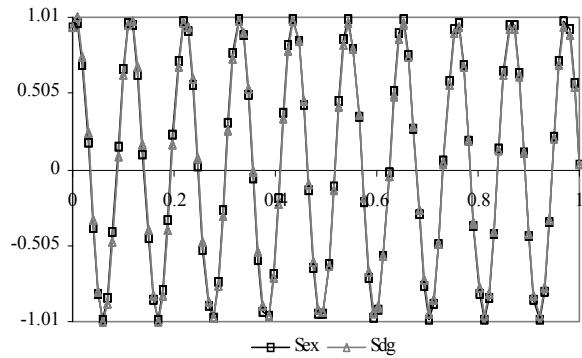
(a) Galerkin FE solution



(b) Discontinuous FE solution



(a) Galerkin FE solution



(b) Discontinuous FE solution

Figure 11. Solution of homogeneous problem in two dimension for sections $x=0.505$ (case a) and $y=0.505$ (case b), $k^2=4000$, $\theta=(3\pi/8)$.

5. CONCLUSIONS

We presented a discontinuous finite element method for the Helmholtz equation, in which the standard finite element space $V^{h,l}$ presents discontinuity of the shape functions across interelement boundaries $V_{DG}^{h,l}$. C^0 continuity is enforced in a weak sense depending on two free parameter β and λ . Optimal values of these parameters are determined numerically by solving a one-dimension homogeneous Helmholtz equation with constant coefficient and

Dirichlet boundary conditions. The numerical results presented in the previous section indicate a good accuracy of the approximate solution of the discontinuous finite element method in one dimension, in which the error is controlled by the magnitude of kh . The accurate of the approximate solution is maintained when the mesh is coarse. For the two-dimensional case, numerical studies of dispersion properties demonstrate the good performance of the discontinuous finite element method. The numerical results presented indicate a good potential of the proposed formulation to solve the Helmholtz problem in the mid and high frequency regime.

Acknowledgements

The authors wish to thank the Brazilian research-funding agencies FAPERJ and CNPq for their support to this work.

REFERENCES

- Babuška, I., Ihlenburg, F., Paik, E.T. and Sauter, S.A., 1995, A generalized finite element method for solving the Helmholtz equation in two dimensions with minimal pollution, *Comput. Methods Appl. Mech. Engrg.*, vol. 128, pp. 325-359.
- Bayliss, C., Goldstein, I. and Turkel, E., 1985, On accuracy conditions for the numerical computation of waves, *J. Comp. Phys.*, vol. 59, pp. 396-404.
- Douglas Jr., J., Santos, J.E., Sheen, D. and Schreiyer, L., 1993, Frequency domain treatment of one-dimensional scalar waves, *Mathematical Models and Methods in Applied Sciences*, vol. 3, No. 2, pp. 171-194.
- Dutra do Carmo, E. G. and Duarte, A. V. C., 2002, New formulations and numerical analysis of discontinuous Galerkin methods, *Computational and Applied Mathematics*, vol. 21, No. 3, pp. 661-715.
- Farhat, C., Harari, I. and Hetmaniuk, U., 2003, A discontinuous Galerkin method with Lagrange multipliers for the solution of Helmholtz problems in the mid-frequency regime, *Comput. Methods Appl. Mech. Engrg.*, vol. 192, pp. 1389-1419.
- Franca, L.P., Farhat, C., Macedo, A.P. and Lesoinne, M., 1997, Residual-free bubbles for the Helmholtz equation, *Int. J. Numer. Methods Engrg.*, vol. 40, pp. 4003-4009.
- Harari, I. and Hughes, T.J.R., 1991, Finite element method for the Helmholtz equation in an exterior domain: Model problems, *Comp. Meth. Appl. Mech. Eng.*, vol. 87, pp. 59-96.
- Harari, I. and Hughes, T.J.R., 1992, Galerkin/least squares finite element methods for the reduced wave equation with non-reflecting boundary conditions in unbounded domains, *Comp. Meth. Appl. Mech. Eng.*, vol. 98, pp. 411-454.
- Ihlenburg, F. and Babuška, I., 1995, Finite element solution of the Helmholtz equation with high wave number Part I: The h-version of the FEM, *Comput. Math. Appl.*, vol. 30, No. 9, pp. 9-37.
- Ihlenburg, F. and Babuška, I., 1997, Finite element solution to the Helmholtz equation with high wave numbers - Part II: the h-p-version of the FEM, *SIAM J. Numer. Anal.*, vol. 34, pp. 315-358.
- Thompson, L.L. and Pinsky, P.M., 1995, A Galerkin least squares finite element method for the two-dimensional Helmholtz equation, *Int. J. Numer. Methods Eng.*, vol. 38, No. 3, pp. 371-397.